



---

## Figures and figure supplements

Cation selectivity of the presequence translocase channel Tim23 is crucial for efficient protein import

**Niels Denkert *et al***

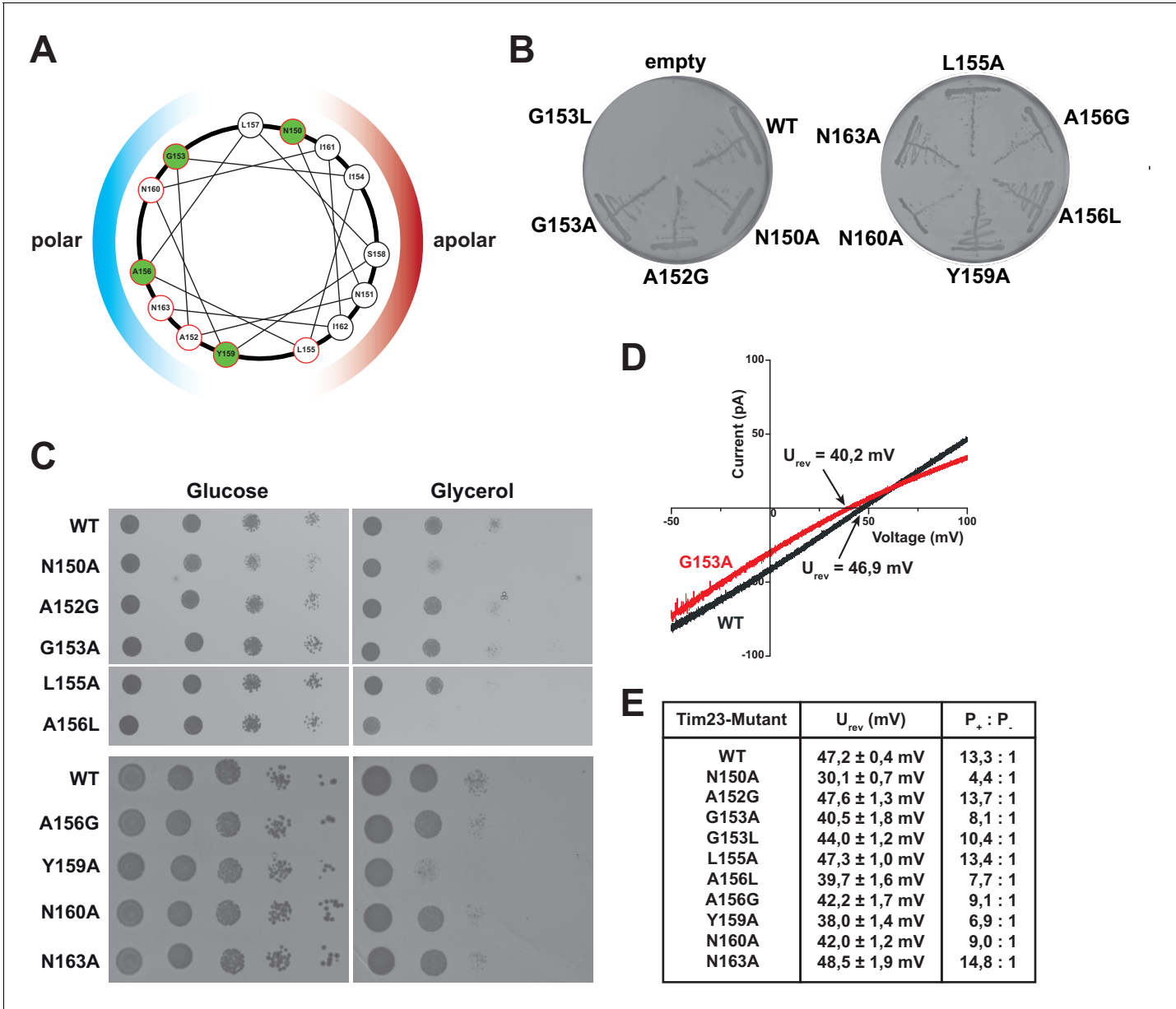


**Figure 1.** Substitutions of pore-lining residues of Tim23 reduce the channel’s ion selectivity and lead to a growth defect in *S. cerevisiae*. (A) Helical wheel projection of amino acid residues 150–163 of the second transmembrane helix of Tim23. Highlighted residues in green indicate near 100% conservation. Colored hemispheres indicates polar/apolar facing regions of helix. Residues mutated in this study are circled in red. (B) *S. cerevisiae* strains with chromosomal deletion of the *TIM23* gene, complemented by a plasmid carrying both *URA3* and *TIM23* gene, were transformed with plasmids containing wild type *TIM23* or mutants and tested for viability after plasmid loss on 5-FOA containing medium. (C) *tim23Δ* yeast cells with plasmids containing wild type *TIM23* or pore-lining mutants were grown on fermentable (left) or non-fermentable (right) media at 37°C. Strains WT to A156L were grown on a single plate each for glucose and glycerol respectively. (D) Electrophysiological current-voltage (I–V) curves were recorded at asymmetrical buffer conditions with 12.5-fold KCl gradient for Tim23 (grey) or Tim23<sup>G153A</sup> (red) to determine reversal potentials. (E) Reversal potentials  $U_{rev}$  were experimentally determined for wild type Tim23 and all mutants by independent triplicates at asymmetrical buffer conditions, the ion selectivity was calculated from the mean reversal potential following the Goldman-Hodgkin-Katz equation. Errors represent standard deviation.

DOI: <https://doi.org/10.7554/eLife.28324.003>

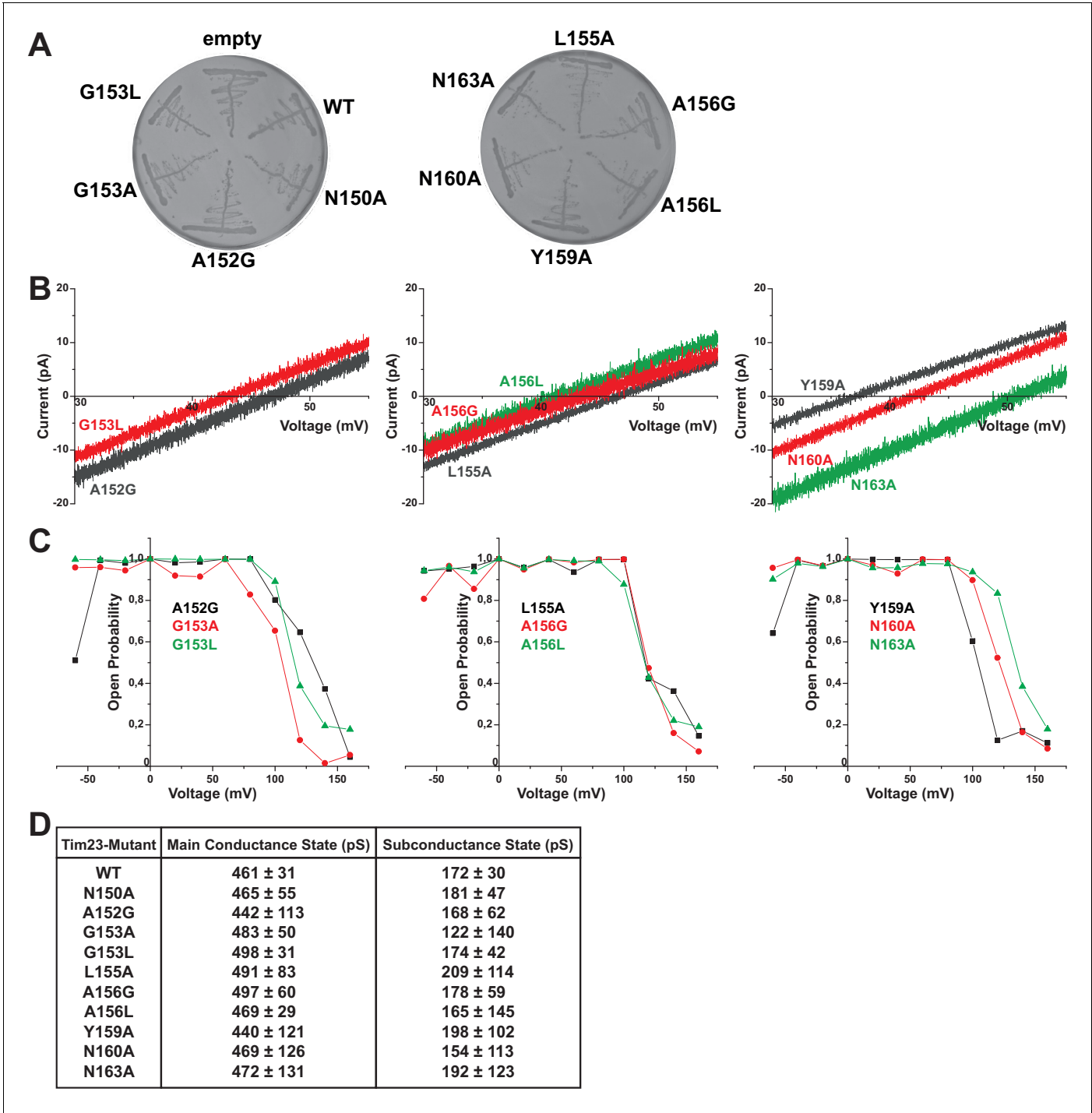
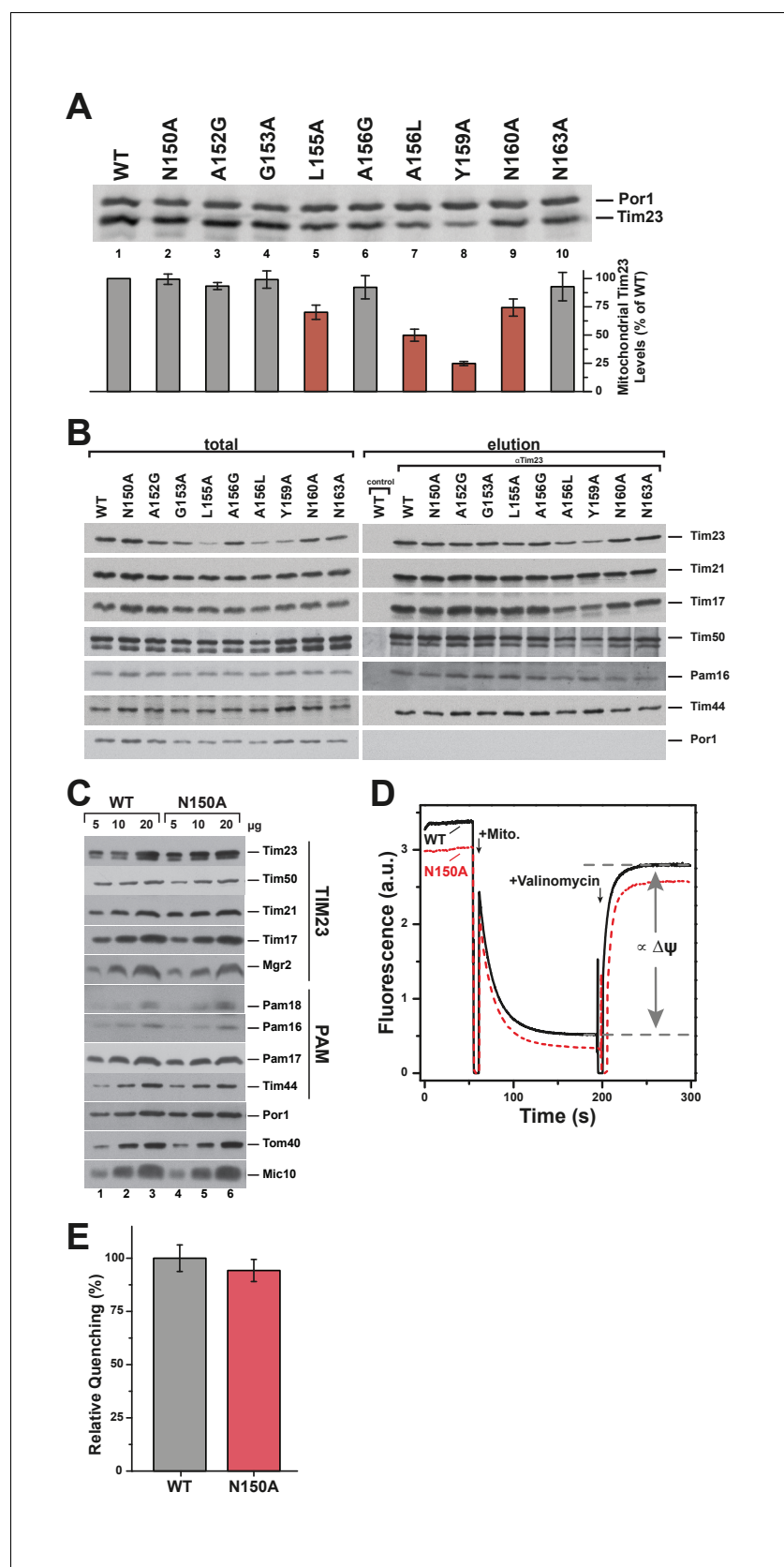


**Figure 1—figure supplement 1.** Electrophysiological screening of Tim23 mutants. (A) *S. cerevisiae* cells with chromosomal deletion of the *TIM23* gene, complemented by a plasmid carrying both *URA3* and *TIM23* gene, were transformed with plasmids containing *HIS3* gene and wild type *TIM23* or mutants. Cells were tested for proper plasmid transformation on -His selective medium. (B) I-V curves of all mutants not shown in Figure 1 or Figure 3. Recorded under asymmetric buffer conditions with 12.5-fold KCl-gradient. (C) Open probabilities of all mutants not shown in Figure 3 were calculated from one full set of constant-voltage recordings (from -60 mV to +160 mV) each. (D) Table of main and primary subconductance states of wild type Tim23 and all mutants were determined by Gaussian fits from gating event histograms (as shown in Figure 3B). Mean and errors represent center and FWHM of Gaussian fits. For Tim23 and Tim23<sup>N150A</sup>, more than 2000 gating events from three independent full sets of recordings and for every other mutant more than 700 gating events from one full set of recordings were analyzed each.

DOI: <https://doi.org/10.7554/eLife.28324.004>

TIM23_HUMAN	MEGGGGSGNKTT-----	12
TIM23_RAT	MEGGGGSSNKST-----	12
TIM23_YEAST	MSWLFGDKTPTDDANAA-----VGGQDTTK-----PKELSLKQS	34
TIM23_DANRE	MDNSTPPPGGFK-----	12
TIM23_NEUCR	MSGLWNTLTGGNKKQQEQQEPAAPAPSAPQTTTTTTSAPSYSPSPFDASQP	50
	*.	
TIM23_HUMAN	GGLA----GF-FGAGGAGYSHADLAG-VPLTGMNPL-SPYLNVDPRYLQ	55
TIM23_RAT	GGLA----GF-FGAGGAGYSNADLAG-VPLTGMNPL-SPYLNVDPRYLQ	55
TIM23_YEAST	LGFEPNINNIISGPG---GMHVDTARLHPLAGLDKG-VEYLDLEEEQLSS	80
TIM23_DANRE	GGLG----SI-FGGGTPEYSNTELSG-VPLTGMSP-SPYLNVDPRYLIQ	55
TIM23_NEUCR	QGVE----AF-LGSS----SFADPTQLHPLAGLNKETLEYISLEDTPLPD	91
	*. : * . . : : **:*:. *::: * .	
TIM23_HUMAN	DTD-EFILPTGANKTRGRFELAFFTIGGCCMTGAAFGAMNGLRLGLKETQ	104
TIM23_RAT	DTD-EFILPTGANKTRGRFELAFFTIGGCCMTGAAFGALNGLRLGLKETQ	104
TIM23_YEAST	LEGSQGLIP-----SRGWTDDL CYGTGAVYLLGLGIGGFSGMMQGLQNIP	125
TIM23_DANRE	DTD-EFILPTGANKTRGRFELAFFTIGGCCITGAAFGTNLNGLRMGLSETR	104
TIM23_NEUCR	AAG-ASVLP-----SRGFTDDL CYGTGITYLTALTIGGAWGLKEGLQRSA	135
	. : :* : ** : : * TMS 2 : * * : **..	
TIM23_HUMAN	NMAWSKPRNVQILNMVTRQGALWANTLGSLALLYSAFGVIEKTRGAEDD	154
TIM23_RAT	SMPWSKPRNVQILNMVTRQGALWANTLGSLALLYSAFGVIEKTRGAEDD	154
TIM23_YEAST	PNSPGKLQLNTVLNHITKRGPFLGNNAGILALSYNIIINSTIDALRGKHDT	175
TIM23_DANRE	DMPWSKPRNVQILNMVTRQGASWANTLGSVALLYSVFGVAIEKARGAEDD	154
TIM23_NEUCR	GQP-PKLRLNSVLNAVTRRGYPYLGNSAGVAICYNLINAGIGYVRGKHDA	184
	. * : : ** : ** : . . * * : * . . * ** . *	
TIM23_HUMAN	LNTVAAGTMTGMLYKCTGGGLRGIARGGLTGLTLTSLYALYNNWEHMKGSL	204
TIM23_RAT	FNTVAAGTMTGMLYKCTGGGLRGIARGGLAGLTLSVYALYNNWEHMKGSL	204
TIM23_YEAST	AGSIGAGALTGALFKSSKGLKPMGYSSAMVAAACAVWCSVKKR-----L	219
TIM23_DANRE	LNTVAAGTLTGMVFKSTGGLKGVARGGIIGLAMSGLYALYNNWDHLKGKS	204
TIM23_NEUCR	ANSILAGALSGMLFKSTRGLKPMMISSGGIVATIAGTWAVARRTF-PSPQF	233
	. : **:::* : * . : ** : : . . : . . . .	
TIM23_HUMAN	LQQSL	209
TIM23_RAT	LQQSL	209
TIM23_YEAST	--LEK	222
TIM23_DANRE	-PSHY	208
TIM23_NEUCR	TNEVD	288

**Figure 1—figure supplement 2.** Sequence conservation of Tim23. Sequence alignment of Tim23 proteins from different species (*Homo sapiens*, *Rattus norvegicus*, *Saccharomyces cerevisiae*, *Danio rerio*, *Neurospora crassa*). Sequence consensus as computed by ClustalW: \* identity; : high similarity; . low similarity. Mutations used in this study are boxed in red.  
DOI: <https://doi.org/10.7554/eLife.28324.005>



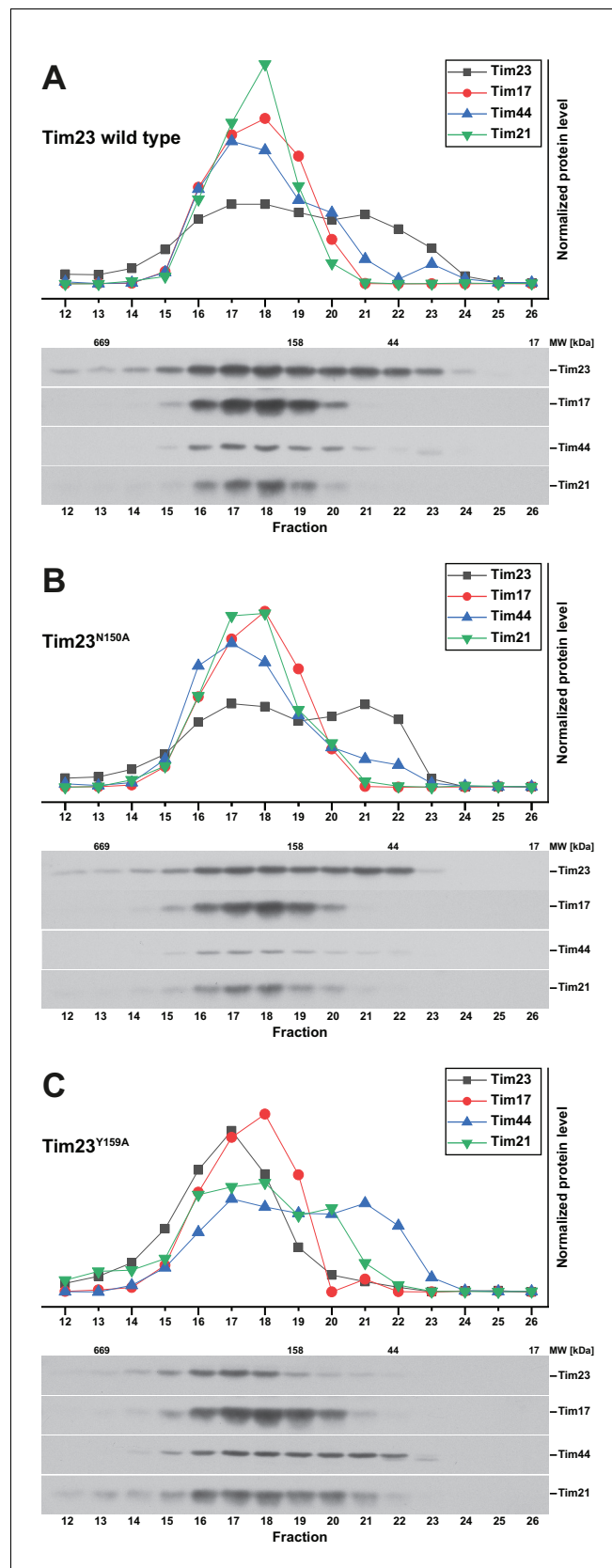
**Figure 2.** Pore-lining mutant Tim23<sup>N150A</sup> is properly expressed and integrated into TIM23 complexes. (A) Mitochondrial steady state levels of yeast expressing wild type Tim23 or mutants were assessed by Western blot

Figure 2 continued on next page

*Figure 2 continued*

analysis (upper) with decoration against Tim23 and Por1 (mitochondrial outer membrane). Protein levels were quantified using fluorescently labelled secondary antibodies in four independent experiments and normalized by mitochondrial Por1 levels. Significantly reduced levels are indicated in red. Error bars represent standard error of the mean. (B) TIM23 complex integrity and recruitment of PAM complex of wild type and Tim23 mutants was examined by co-immunoprecipitation of mitochondrial lysates using Tim23 antibodies. (C) Isolated mitochondria containing Tim23 or Tim23<sup>N150A</sup> were Western blotted and decorated against proteins of the TIM23 complex, the PAM complex, Por1 and Tom40 (both mitochondrial outer membrane) and Mic10 (mitochondrial inner membrane). (D) Membrane potential  $\Delta\Psi$  was assessed by adding isolated mitochondria containing Tim23 (black solid) or Tim23<sup>N150A</sup> (red dashed) to the fluorophore DiSC<sub>3</sub>(5), then dissipating  $\Delta\Psi$  with valinomycin and determining the amount of quenching. Grey dashed lines and arrows indicate the parameter quantified in (E). (E) Relative fluorophore quenching as a measure of membrane potential  $\Delta\Psi$  for Tim23 (grey) and Tim23<sup>N150A</sup> (red) was quantified (as depicted in D) in three independent experiments. Error bars represent standard error of the mean before normalization.

DOI: <https://doi.org/10.7554/eLife.28324.006>



**Figure 2—figure supplement 1.** TIM23 complex characterization by size exclusion chromatography profiles. (A) – (C) Relative elution profile of the TIM23 complex (top) was assessed by quantification of Western blots (bottom)

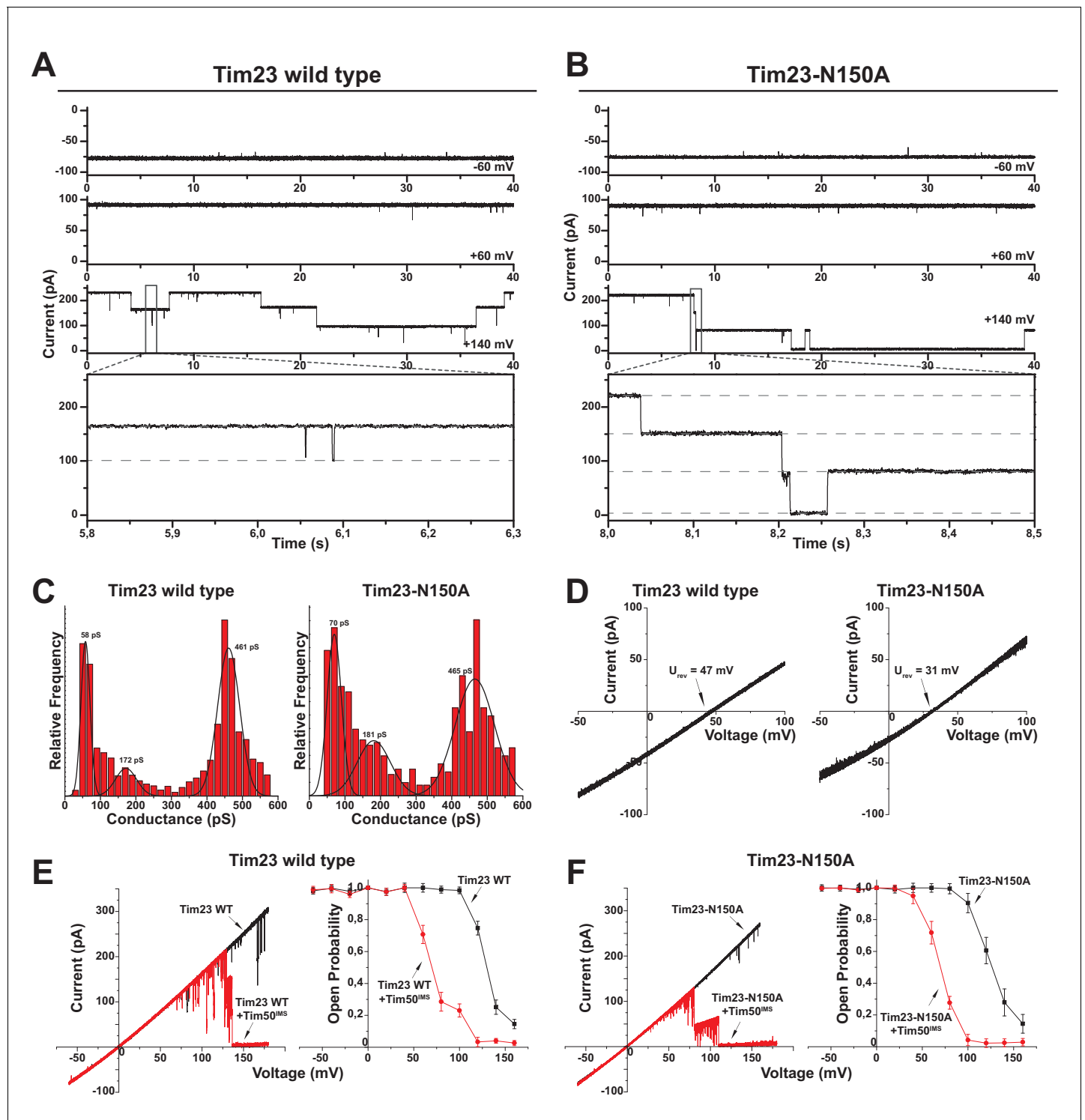
Figure 2—figure supplement 1 continued on next page

Figure 2—figure supplement 1 continued

after size exclusion chromatography of solubilized mitochondria containing Tim23 wild type (A), Tim23<sup>N150A</sup> (B) and Tim23<sup>Y159</sup> (C).

DOI: <https://doi.org/10.7554/eLife.28324.007>





**Figure 3.** Tim23<sup>N150A</sup> displays reduced cation preference. (A)/(B) Tim23- (A) or Tim23<sup>N150A</sup>-containing (B) proteoliposomes were fused with planar lipid bilayers and single-channel activity was characterized by electrophysiological current recordings. (C) Gating event histograms for Tim23 (left) and Tim23<sup>N150A</sup> (right) were calculated from constant-voltage recordings (as depicted in A) with at least 2000 gating events each. The three most prominent classes of conductance changes were modeled with a Gaussian fit. (D) I-V curves at asymmetrical buffer conditions were recorded for Tim23 (left) and Tim23<sup>N150A</sup> (right) with indicated reversal potential  $U_{rev}$  for 12.5-fold KCl-gradient. (E)/(F) I-V curves (left) and open probabilities (right) were determined for bilayer incorporated Tim23 (E) or Tim23<sup>N150A</sup> (F) before (black) and after (red) addition of 700 nM Tim50<sup>IMS</sup> to IMS-side of the channel. Error bars represent standard deviation (SD,  $n = 3$ ).

DOI: <https://doi.org/10.7554/eLife.28324.008>

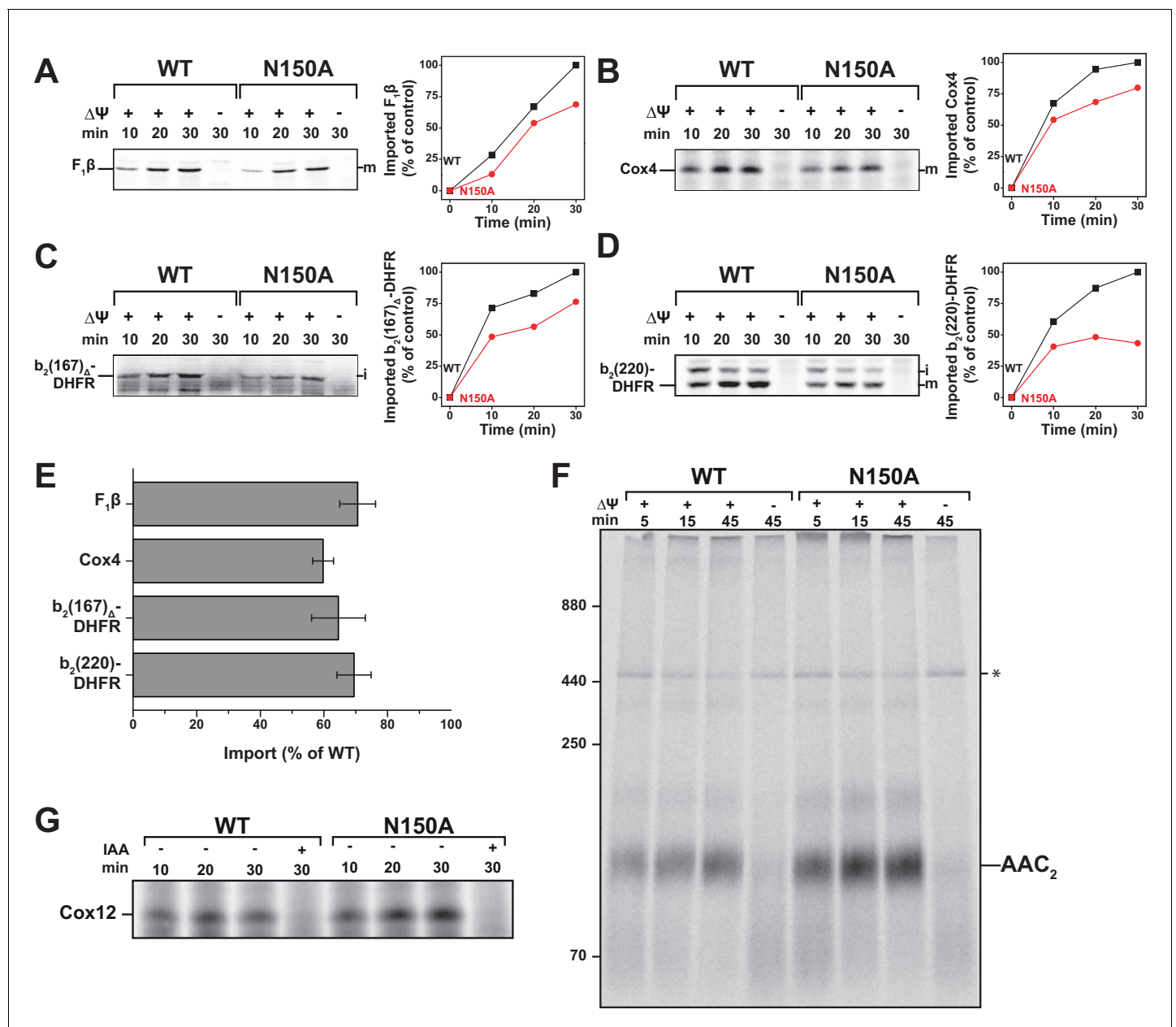


**Figure 4.** Tim23<sup>N150A</sup> exhibits significant import defects for various TIM23 substrates. (A–D) Import capability of wild type and tim23<sup>N150A</sup> mutant mitochondria was determined by incubating [<sup>35</sup>S]-radiolabeled matrix destined precursors F<sub>1</sub>β (A), Cox4 (B), b<sub>2</sub>(167)<sub>Δ</sub>-DHFR (C) or the inner membrane sorted b<sub>2</sub>(220)-DHFR (D) with isolated mitochondria for 10, 20 or 30 min. The import reactions were stopped by dissipating  $\Delta\Psi$  and subsequent Proteinase K (PK)-digest. Digital autoradiographs (left) were analyzed and quantified (right). Maximum import into wild type mitochondria was set to 100%. (E) Relative import efficiency after 15 min of import into mitochondria containing Tim23<sup>N150A</sup> was quantified for different substrates. Error bars represent standard error of the mean (SEM, n = 3). (F) Carrier import into Tim23<sup>N150A</sup>-containing mitochondria was assessed via ADP/ATP carrier (AAC) complex assembly by incubating [<sup>35</sup>S]-radiolabeled AAC with isolated mitochondria for 15, 30 or 45 min. The import reaction was stopped by dissipating  $\Delta\Psi$  and subsequent PK-digest. Assembly of AAC dimer was monitored by BN-PAGE. (G) The MIA substrate Cox12 was [<sup>35</sup>S]-radiolabeled and imported into Tim23<sup>N150A</sup>-containing mitochondria for 10, 20 or 30 min. The import reaction was stopped by addition of iodoacetamide (IAA) and subsequent PK-digest.

DOI: <https://doi.org/10.7554/eLife.28324.009>

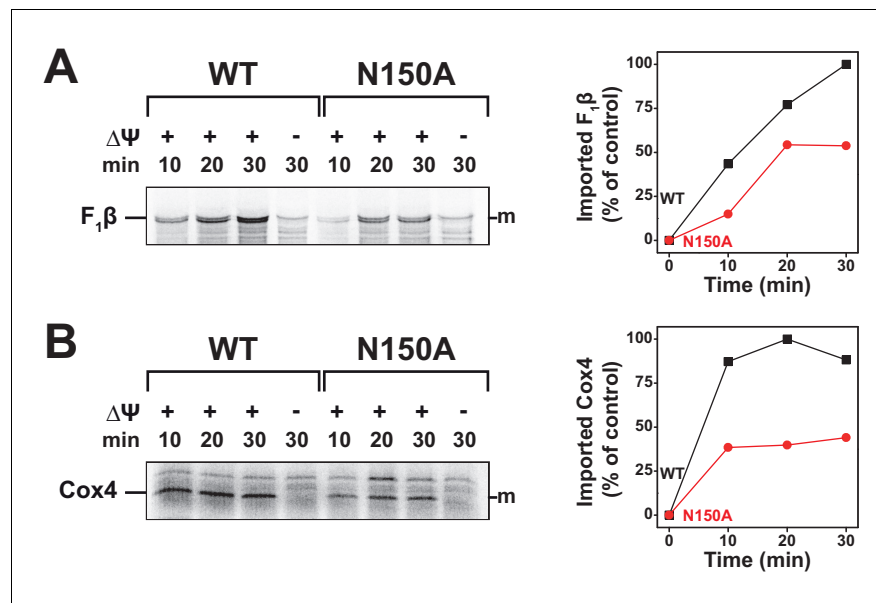


**Figure 4—figure supplement 1.** Import of TIM23-substrates at non-permissive temperatures. (A and B) Temperature influence on import capability of Tim23<sup>N150A</sup> was assessed by incubating [<sup>35</sup>S]-radiolabeled  $F_1\beta$  (A) or Cox4 (B) with isolated mitochondria for 10, 20 or 30 min at 37°C. Maximum import into wild type mitochondria was set to 100%.

DOI: <https://doi.org/10.7554/eLife.28324.010>

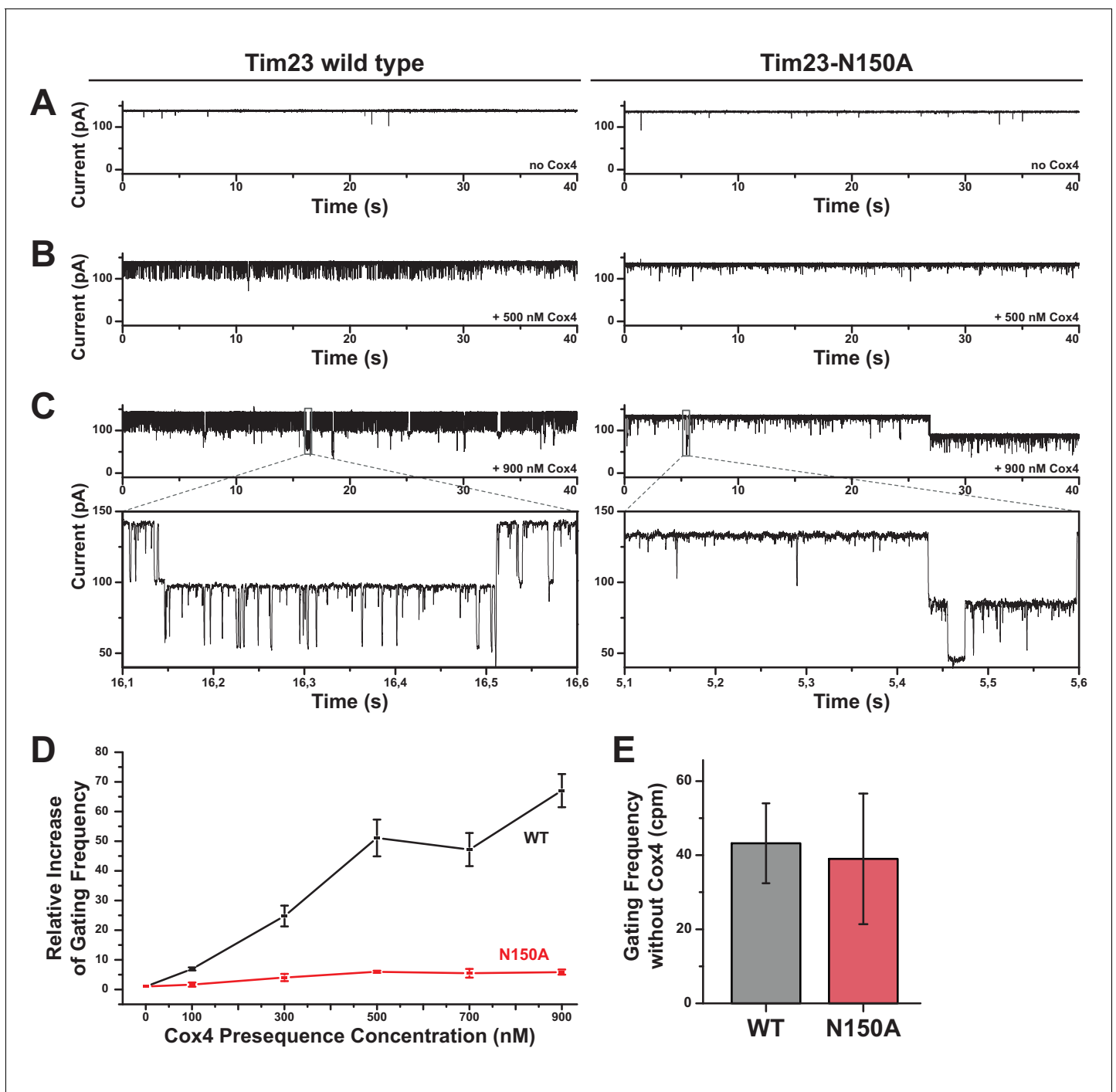


**Figure 5.** Increased gating frequency as a measure of channel response to presequence titration is heavily reduced for Tim23<sup>N150A</sup>. (A) Bilayer-incorporated Tim23 (left) or Tim23<sup>N150A</sup> (right) single-channel currents were recorded at +80 mV before addition of Cox4 presequence peptide. (B)/(C) Current recordings of wild type (left) and mutant (right) channels were performed after each titration step. (D) Channel response of Tim23 (black) and Tim23<sup>N150A</sup> (red) after addition of Cox4 presequence was quantified by counting gating events and calculating the relative increase in activity compared to unstimulated channels. Error bars represent standard deviation. (E) Absolute gating frequency of unstimulated Tim23 and Tim23<sup>N150A</sup> was determined from current recordings before presequence titration. Error bars represent standard deviation (SD, n = 3).

DOI: <https://doi.org/10.7554/eLife.28324.011>